European Journal of Wood and Wood Products (2019) 77:903–917
https://doi.org/10.1007/s00107-019-01441-8

ORIGINAL

Quantifying knots by image analysis and modeling their effects on the mechanical properties of loblolly pine lumber

Stephen Wright[1] · Joseph Dahlen[1] · Cristian Montes[1] · Thomas L. Eberhardt[2]

Received: 7 November 2018 / Published online: 31 July 2019
© Springer-Verlag GmbH Germany, part of Springer Nature 2019

Abstract
Automated grading machines that quantify knots are increasingly deployed by lumber mills, however their use in mill studies that assess lumber quality have been limited. The objective here was to develop a method to evaluate the knots of loblolly pine lumber using image analysis and to develop models to predict modulus of elasticity (MOE) and modulus of rupture (MOR) from 171 pieces of dimension lumber. Lumber was photographed on the wide faces and individual knots were identified using the *k*-means clustering algorithm. The percentage of wood made up of knots on the wide faces (Knot%) was calculated by summing the individual knot areas over the total surface area, as well as on a sub-section of the lumber span which was optimized separately for MOE ($Knot\%_{MOE}$) and MOR ($Knot\%_{MOR}$). Models were built using the knot measurements and compared to models built using specific gravity (SG) and acoustic velocity squared (AV^2). Knot% explained 30% of the variation in MOE and 39% of the variation in MOR. Incorporating $Knot\%_{MOE}$ into a model with SG and AV^2 did not appreciably improve model performance ($R^2 = 0.75$, RMSE = 1.1 GPa) over the base SG and AV^2 model ($R^2 = 0.74$, RMSE = 1.2 GPa). Incorporating $Knot\%_{MOR}$ into a model with SG and AV^2 significantly improved the prediction ($R^2 = 0.65$, RMSE = 7.2 MPa) compared to the base SG and AV^2 model ($R^2 = 0.56$, RMSE = 8.0 MPa). This study demonstrates the feasibility of using image analysis to assess knot information in lumber to improve predictions of mechanical properties.

1 Introduction

The southeastern United States has become one of the most important regions for softwood lumber production due to the abundant raw material availability of southern pine that was established through extensive forestation of abandoned agricultural fields (Schultz 1999; Wear and Greis 2002; Fox et al. 2007). The major southern pines consist of loblolly (*Pinus taeda*), slash (*Pinus elliottii*), longleaf (*Pinus palustris*), and shortleaf (*Pinus echinata*) pines (South and Harper 2016). The region's timber production doubled between the 1950s and the 1990s, and it now supplies approximately 16% of the world's timber (Wear and Greis 2002). The timber growth increases are the result of a combination of improved genetic material and intensive silvicultural practices (Jokela et al. 2009), which has led to reduced rotation ages as loblolly pine trees reach merchantable size faster than in the past. For example, loblolly trees can obtain sawtimber size (diameter at breast height (DBH) ≥ 31 cm) and chip-n-saw size (23 cm ≤ DBH ≤ 30 cm) by 25 and 16 years of age, respectively (Clark et al. 2008; Vance et al. 2010).

The reductions in rotation age have resulted in a larger proportion of corewood (juvenile wood) in the merchantable trees (Burdon et al. 2004; Moore and Cown 2017). Corewood, starting from the pith, and laid down outward, is the wood formed in young trees, while outerwood is formed later on as the tree matures (Burdon et al. 2004; Lachenbruch et al. 2011). Corewood is characterized by lower stiffness and strength, and higher longitudinal shrinkage, compared to outerwood (Ying et al. 1994; Larson et al. 2001). In loblolly pine, the low stiffness and strength of corewood is the result of low specific gravity (SG) (wood density divided by water density) and high microfibril angle (MFA), especially for the growth rings near the pith (Burdon et al. 2004; Cramer et al. 2005; Jordan et al. 2007; Clark et al. 2008). As a consequence of the changes that have occurred in southern pine wood quality, in 2013, the engineering design values for visually graded southern pine lumber were reduced

✉ Joseph Dahlen
jdahlen@uga.edu

[1] Warnell School of Forestry and Natural Resources, University of Georgia, 180 E Green Street, Athens, GA 30602-2152, USA

[2] Forest Products Laboratory, US Forest Service, One Gifford Pinchot Drive, Madison, WI 53726, USA

to address the lower mechanical properties of the lumber being produced and available in commerce (ASTM D1990 2016; Butler et al. 2016). For example, in the No. 2 grade, the design values for MOE were reduced from 11.0 GPa to 9.7 GPa and MOR values reduced from 10.3 to 7.6 MPa in the 2×4 size (38.1 mm×88.9 mm).

For loblolly pine, much of the work examining the impact of silviculture and genetics on wood and fiber quality has focused on the physical properties, specifically wood SG, with some work done on the anatomical properties. Changes to branching, and thus the frequency and size of knots in the resultant lumber, have been given little attention. Lumber failure occurs at the weakest cross section relative to the test setup, which is often at a knot or near knots because of severe grain deviations around the knots (Madsen 1992; Hu et al. 2018a). Recent technological advancements have made the rapid measurement of knots feasible. Knots have been imaged using single pass X-ray scanners where knot zones are detected on the wide face, and their corresponding depths determined by the penetration of the X-rays through to the detector(s) beneath (Schajer 2001; Oh et al. 2008, 2009). In a study by Schajer (2001), a single pass X-ray scanner was used to measure wood density of southern pine lumber, with the knots identified by their higher density. Material for the study was acquired from 3 mills, with 2 mills sampled from Arkansas (N = 311, N = 136), and 1 mill sampled from Mississippi (N = 158). Schajer (2001) found that predicted lumber strength, based on a wood structural factor accounting for localized density, increases from knots, and linear models were able to explain 57%, 65%, and 69% of the variation in the modulus of rupture (MOR) determined from bending tests of samples from the 3 different mills. Oh et al. (2008), again using a single pass X-ray scanner, found that the ratio between the moment of inertia of the knot to the full cross section explained 65% of the variation in MOR using a linear model for 141 pieces of Japanese larch (*Larix kaempferi*).

The quantification of knots is increasingly done via measurement of the "tracheid effect", whereby a camera, in conjunction with a series of lasers, is used to measure localized wood fiber orientation changes within the wood due to knots (Roblot et al. 2010; Briggert et al. 2018). In contrast to the X-ray measurement of knots, measuring knots via the tracheid effect offers the advantage of capturing distinct information on all four sides of the lumber. Roblot et al. (2010) used the tracheid effect to detect knots in Douglas-fir (*Pseudotsuga menziesii*) (N = 226) and Norway spruce (*Picea abies*) (N = 225) dimension lumber. From projections of the knots into the lumber, from all 4 surfaces, they calculated the knot area ratio, which corresponds to the cross-sectional area of the knot(s) divided by the total cross-sectional area of the lumber in the same plane. Predicting MOR using a multiple regression linear model from knot area ratio and modulus of elasticity (MOE) determined dynamically explained 55% of the variation in MOR for Norway spruce and 70% of the variation for Douglas-fir. Olsson et al. (2013) calculated localized wood fiber orientation using the tracheid effect and combined this information with measurements of dynamic MOE for Norway spruce (N = 105). They found that their model explained 71% of the variation in MOR, an improvement from the coefficient of determination of 59% when predicting MOR from dynamic MOE alone. Using both X-ray information and the tracheid effect, Viguier et al. (2017) examined 437 samples of Norway spruce and 805 samples of Douglas-fir. They found that predicted MOE explained 79% (Norway spruce) and 75% (Douglas-fir) of static MOE, and predicted MOR explained 68% (Norway spruce) and 58% (Douglas-fir) of MOR.

Recent changes in design values for southern pine lumber, in conjunction with a wider implementation of intensive silviculture practices, have increased the need to evaluate the raw material supply chain to further understand the mechanical properties of lumber being produced. While the use of commercial scanning equipment via X-rays and/or the tracheid effect can provide accurate knot quantifications, most laboratories do not have access to the equipment and thus there is a need to develop alternative methods for knot quantification that can be readily implemented in a laboratory setting. These methods need to improve on the manual measurement techniques that typically evaluate knots following testing to failure (França et al. 2018). Recent work has characterized knots in Douglas-fir veneers using image analysis (Todoroki et al. 2010); it appeared feasible that an adaptation of the technique could be an effective method for measuring the knots in lumber. The objectives of this study were to (1) test the feasibility of using image analysis to identify and quantify knots in loblolly pine lumber, and (2) develop models between MOE and MOR with transformations of knot areas on selected lumber surfaces, and compare the results to models developed using SG and acoustic velocity. Characterization of knots using image analysis, which is of much lower capital investment than the use of an X-ray or laser (tracheid effect) equipment, could lead to more studies investigating the relationships between knots in lumber and silviculture practices, thereby leading to improved forest management decisions.

2 Materials and methods

2.1 Lumber source

Trees used in this study were harvested from intensively managed stands in the United States southeast lower coastal plain, near Brunswick, Georgia. Further details on the sampling protocol can be found in Butler et al. (2016; 2017) and Dahlen

et al. (2018). Trees were felled, delimbed, and bucked into 5.2 m logs in the woods prior to transport to the participating mill (Hoboken, GA, USA) where the logs were sawn into dimension lumber, kiln-dried to a target moisture content of 15% to ensure each piece was less than 19%; the lumber was then planed and graded into the No. 1, No. 2, and No. 3 grades according to the visual grading rules for southern pine (ASTM D245-11 2011; SPIB 2004, 2014). Following processing, the lumber was transported to the Wood and Fiber Quality Laboratory at the University of Georgia in Athens, GA, USA. A subset of the lumber was included for this study as follows: 72 pieces of 2×6 nominal lumber (38.1 mm×139.7 mm) with 13 pieces graded as No. 1, and 59 pieces graded as No. 2; 99 pieces of 2×8 nominal lumber (38.1 mm by 184.2 mm) with 59 pieces graded as No. 1, and 40 pieces graded as No. 2.

2.2 Lumber image collection and testing procedures

The lumber was prepared and tested in a laboratory with conditions that were typically near 24 °C and 55% RH. Prior to trimming the lumber to approximate test span dimensions, the strength reducing defect was predicted by visually inspecting each piece, with an emphasis placed on identifying the largest knot and including it randomly in the test span (ASTM D4761 2013). The lumber was then trimmed to the 17 to 1 span to depth ratio plus an allowance for overhang on the reaction points. The SG of the lumber was calculated using the measured weight and dimensions, and moisture content was determined using a handheld moisture meter calibrated to southern pine (Wagner Meter, Rogue River, OR, USA). The mean lumber moisture content was 11.2%. The measured SG values were then adjusted to 15% moisture content (oven dry weight, volume at 15% moisture content) using a volumetric shrinkage rate of 12.3% (Glass and Zelinka 2010) to correspond to the 15% moisture content used for the mechanical properties (ASTM D1990 2016). The longitudinal acoustic velocity was measured using the Fakopp Portable Lumber Grader (PLG) (AV_{PLG}) (Fakopp BT, Agfalva, Hungary) which calculates the acoustic velocity (m s^{-1}) using the first harmonic frequency of a resonant wave (Wang 2013):

$$AV = 2f_0L \tag{1}$$

where AV is weighted mean acoustic velocity (m s^{-1}), f_0 is the first harmonic frequency of an acoustic wave signal (Hz) and L is the length (m) of the material (Wang 2013). The AV term is squared in the calculation of dynamic MOE:

$$MOE_{dyn} = \rho AV^2 \tag{2}$$

where MOE_{dyn} is dynamic MOE determined using wood density (ρ) and AV (Wang 2013); thus the results here are reported as AV^2 with units of $km^2\ s^{-2}$.

Because the intent of this project was not to develop an instrument for automatically grading lumber in a commercial setting, but was instead to determine the impact that knots have on the mechanical properties of lumber, the knotty regions were delineated from clearwood by filling in the knots using a black marker. This was a straightforward operation since southern pine has knots that are very easy to delineate from clearwood upon visual inspection. Each piece of lumber was then photographed in color (RGB) on the wide faces using a Nikon D300 12.3 megapixel camera with a Nikon 12–24 mm wide angle lens (Tokyo, Japan). The camera was set at a fixed position on a tripod and the lumber placed on a table with end and side stops such that each piece was in the same position relative to the camera. The lighting was a combination of the building lighting plus the flash from the camera. The narrow faces of the lumber were not photographed and thus the technique mimics the aforementioned single pass X-ray measurements used to quantify knots (Oh et al. 2008). Each piece had a unique number, which was used to manually pair the two images with the rest of the data.

Each piece of lumber was then tested in static edgewise destructive bending (ASTM D4761 2013; ASTM D198 2015) using a four-point bending setup in "third-point" loading (load heads positioned one third of the span distance from the reactions) on a universal testing machine. The span-to-depth ratio was 17:1 (2×6: 2375 mm to 140 mm, 2×8: 3131 mm to 184 mm). The MOE was determined from the displacement of the lumber caused by the applied load in the linear region, with the linear displacement measured at mid-span. The formula for MOE is:

$$MOE = \frac{23PL^3}{108bd^3\Delta} \tag{3}$$

where P is the change in load between two load points in the linear region, L is the span, b is the base of the beam, d is the depth of the beam, and Δ is the change in deflection corresponding to the two load points (ASTM D198 2015). It is noted that the ASTM D198 (2015) standard does not discuss global or local MOE terminology, however the MOE method and calculation is equivalent to global MOE method as described by Olsson et al. (2012):

$$MOE = \frac{PL^3}{bd^3\Delta}\left[\left(\frac{3a}{4L}\right) - \left(\frac{a}{L}\right)^3\right] \tag{4}$$

where the terms in Eq. (4) are the same as in Eq. (3) with the addition of *a*, which is the distance between a support and the nearest load point. Because the setup was in third-point loading, *a* is equal to one third of L, thus Eq. (4) simplifies to Eq. (3) when substituting one third of L for *a*. The MOR was determined from the total amount of load applied at the moment of failure using:

$$MOR = \frac{P_{max}L}{bd^2} \tag{5}$$

where P_{max} is the maximum load. Following testing, the length to failure and type of failure (tension, compression, shear, and combination) were recorded. The mechanical properties were adjusted to 15% moisture content (Evans et al. 2001; ASTM D1990 2016; Butler et al. 2016).

2.3 Image analysis

The image analyses were done in the R statistical software environment (R Core Team 2018) and the Python programming language version (Python Software Foundation, https://www.python.org/). R was used with the RStudio interface (RStudio 2018) and the packages maps (Brownrigg 2016), raster (Hijams 2016), rgdal (Bivand et al. 2017), rgeos (Bivand and Rundel 2017), sp (Pebesma and Bivand 2016), and the tidyverse series of packages (Wickham and RStudio 2017). Python 3.6 was used with the packages NumPy (Oliphant 2006), opencv (Bradski 2000), pandas (McKinney 2010), and scikit-image (skimage) (van der Walk et al. 2014).

The following steps were carried out in R (R Core Team 2018). The original RGB image, which included some background information, was cropped to roughly correspond to the region of interest. A white mask was then applied to isolate the lumber from the background information that could not be removed during the rough cropping procedure. Both the rough cropping and the white mask were applied manually. Contrast stretching was done for each channel of the RGB image to equalize the contrast across the piece:

$$\text{intensity} = \frac{\text{intensity}-\text{min}}{\text{max}-\text{min}} \times 255 \quad (6)$$

where intensity is the value ranged from 0 to 255, min is the minimum intensity for the image, and max is the maximum intensity of the image. *K*-means clustering was then used to separate the knotty regions within the lumber, which works by classifying the intensity of light for each pixel information, ranging from 0 to 255 for 8-bit images for each color channel of the RGB image, into a limited number of intensity values, which corresponds to the number of clusters selected (Hartigan and Wong 1979; Kanungo et al. 2002). Because the algorithm incorrectly identified some regions of the lumber that were not knots, a manual identification of the correct knot clusters was done to ensure that the selected areas were actual knots. Following the manual confirmation of the knots, the color of the knots on the images were changed to red, such that further identification of knots could be automatic, and the images then saved.

The following steps were then carried out in Python (Python Software Foundation, https://www.python.org/) on the images that were saved as described above. Because camera lenses have distortion, and to correct any misalignment between the focal plane of the lens and the lumber piece, the image distortion was corrected by applying a projective transformation, which identified the corner coordinates of each image and stretched them to the undistorted coordinates; the procedure is described in Hartley and Zisserman (2003) and in the documentation for the scikit-image library (van der Walk et al. 2014). For each lumber piece, images were collected on the two wide faces. The second image for each piece was flipped on the horizontal axis such that the knots were correctly aligned between the compression and tension testing faces. The *k*-means clustering algorithm was again run and then the knot size and position were determined. The number of *k*-means clusters selected varied between pieces so that the best cluster could be chosen for each piece to allow for optimal separation of the knots from the clearwood. The location of the lumber failure was converted from centimeters to pixels and then the location failure was plotted onto each image as line perpendicular to the main axis.

2.4 Data analyses

The statistical analyses and associated graphics were done in the R statistical software environment (R Core Team 2018) with the RStudio interface (RStudio 2018), the gridExtra (Auguie 2016) package, and the tidyverse series of packages (Wickham and RStudio 2017).

The list of knots, with their locations and sizes, was used to calculate the percent of the piece that was composed of knots. Knots from the entire piece, including the overhang past the reaction points, were first considered in three ways. The first was based on the grading rules, which considers the width of the knot and not the length of the knot (SPIB 2004; ASTM D245 2011). The sum of the knot widths were compared to the width of the piece ($\text{Knot\%}_{\text{Width}}$):

$$Knot\%_{Width} = \frac{\sum Knot_{Width}}{Width} \times 100 \quad (7)$$

where the sum of the knot widths ($\text{Knot\%}_{\text{Width}}$) from both faces was compared to the overall width of the piece. The second method used the actual area of the knots (Knot%) by calculating the actual area of each knot in pixels, then summing these areas and dividing by the total lumber area, in pixels, of the two wide faces. The third method used the rectangular area of the knots ($\text{Knot\%}_{\text{Rectangle}}$), which was calculated by the minimum and maximum X (length) and Y (width) pixel values, and then summing these areas and dividing by the total lumber area, in pixels, of the two wide faces. Where appropriate, the pixel values were converted to metric dimensions to generate summary statistics for the knot sizes. For the three knot percentage measurements ($\text{Knot\%}_{\text{Width}}$, Knot%, $\text{Knot\%}_{\text{Rectangle}}$), a square root transformation was applied to improve linearity between the knot measurement and MOE or MOR. Correlations between

variables were calculated and the knot percentage measurement that had the highest correlation to MOE and MOR was selected for further analysis.

The bending test uses a four-point bending setup in "third-point" loading where the load heads are positioned one third of the span distance from the reaction points and thus the region with the highest stress is in between the load heads. Here 74% of the pieces failed in between the two load heads (Butler et al. 2016). Because not every piece fails in between the load heads, the question arises as to how much influence knots outside of the load heads have on MOE and MOR. It is hypothesized that knot frequency and size would influence MOR in a narrower distance over the total span than MOE since failure is common at a single knot or a combination of knots. Failure is also associated with being close to or directly under the load heads. To determine this effect, a knot percentage calculation was conducted that included knots in between the load heads (33% of the span), and then iteratively increased the distance until the full span was accounted for (100% of the span), where the distance increased outside the load heads by one half percent each iteration. A linear model explaining the effect of each of the knot percentages, at each iteration, was run for MOE and MOR.

The wood failure location was plotted onto each image and the type of failure was examined for each piece (tension, compression, and shear). This information was used to classify the cause of the failure into one of three categories as follows: clear wood, failure as a result of a single knot, and failure as a result of a combination of knots. Pieces that failed in shear were classified as clearwood failures. Summary statistics were calculated for each wood property variable for the overall dataset and for the different causes of failure. Analysis of variance (ANOVA) at a 0.05 significance level was used to determine significant differences in the means of the different variables with mean separation done using Tukey's test.

Linear and multiple linear regression models were constructed to determine the relationship between the dependent variables (MOE and MOR) with the independent variables (knot percentage, SG, AV^2, MOE_{dyn}). Models were compared between using MOE_{dyn} calculated using Eq. (2), versus the performance of models fit using both the individual SG and AV^2 variables. Model fit was evaluated using the coefficient of determination (R^2) and the root-mean-square-error (RMSE) and between model performance was determined using ANOVA. Because SG and AV^2 are relatively easy to measure on lumber pieces, a multiple regression model including SG and AV^2 was used as the baseline model to determine whether including knot percentage values would significantly improve the model results, and thus whether the knot percentage values determined here are worthwhile measurements above and beyond SG and AV^2. The same comparison was conducted using MOE_{dyn} instead of using the SG and AV^2 parameters separately.

3 Results and discussion

3.1 Optimization of knot area ratio measurements and correlations between variables

Figure 1 shows four images of the same sample, two for each of the wide faces photographed. The two grayscale images (converted from RGB) show the knots identified in black on each face with the vertical line illustrating the location of the failure after mechanical testing. For illustration purposes, the binary (black and white) images show the knots completely delineated from the rest of the wood. Figure 2 shows a closer view of a section of the same sample illustrated in Fig. 1, which demonstrates the effect of the *k*-means algorithm in grouping the pixels into a limited number of clusters. For identifying the knots on the grayscale images, the number of *k*-means clusters depended on the specific image with the median number of clusters used being 6, but some images required 7 or 8 clusters to properly allow for separation of the knots from the clear wood. The correlations between the three knot measurements were strong (Table 1), with Knot% vs. $Knot\%_{Rectangle}$ having the highest correlation ($R = 0.98$). Knot% had slightly higher correlations to MOE ($R = -0.55$ versus -0.54) and MOR ($R = -0.63$ versus -0.62) than $Knot\%_{Rectangle}$, with both having higher correlations to MOE

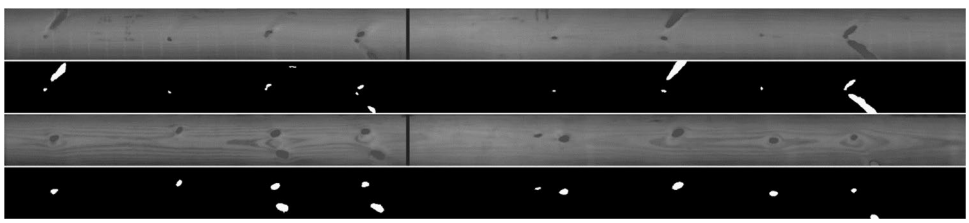

Fig. 1 Example images showing the two wide faces of a single piece of 2×6 nominal lumber. The grayscale images show the knots identified using the *k*-means clustering algorithm, and the black vertical line indicates where the failure occurred. The binary (black and white) images show the knots (white) isolated from the rest of the piece (black)

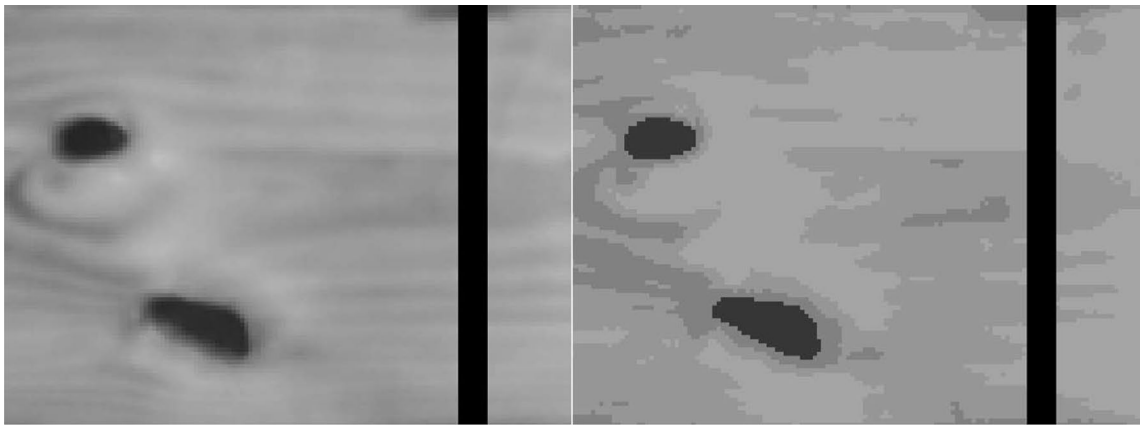

Fig. 2 Closer view of section from Fig. 1 with the black line indicating failure location and pasted onto the image. The left image shows the grayscale image with the knots marked with black marker, and the right image shows the knots identified using the *k*-means clustering algorithm

Table 1 Pearson correlation matrix among measures of knots and modulus of elasticity and modulus of rupture, all coefficients were statistically significant ($\alpha < 0.05$)

Property	Knot%	$Knot\%_{Rectangle}$	MOE	MOR
$Knot\%_{Width}$	0.86	0.88	−0.46	−0.53
Knot%		0.98	−0.55	−0.63
$Knot\%_{Rectangle}$			−0.54	−0.62

$Knot\%_{Width}$ percentage of knots determined from the width of the knots, *Knot%* percentage of area with knots determined using the actual area of the knots, *$Knot\%_{Rectangle}$* percentage of area with knots determined using the rectangle area of the knots, *MOE* static modulus of elasticity, *MOR* modulus of rupture

Table 2 Summary statistics of number and size of knots in lumber

Property	Lumber Dimension	Mean	Standard deviation	Quantile	
				25th	75th
Number of knots	2×6	16	5	13	20
	2×8	22	7	17	25
	Overall	20	7	15	24
Knot Size (cm^2)	2×6	4.7	6	0.9	6.0
	2×8	6.0	8	1.2	7.4
	Overall	5.6	7.4	1.1	7

and MOR than $Knot\%_{Width}$. Based on these results, Knot% was used during the modeling and optimization efforts which is the knot measurement using the actual area of the knots.

Table 2 shows the summary statistics of the knots overall and by lumber nominal dimension. On average, the number of knots were more numerous for the 2×8 lumber (N = 22), and larger (mean = 6 cm^2), than for the 2×6 lumber (N = 16, mean = 4.7 cm^2), which was expected because larger lumber nominal dimensions have longer test spans and larger allowable knot sizes with a given grade. The standard deviation for knot size was quite high (7.4 cm^2), which demonstrates that knot sizes are highly variable in loblolly pine lumber with some knots being quite large, whereas other knots are quite small.

The correlations between variables are shown in Table 3, and the results of optimizing the measurement of Knot% for MOE and MOR are shown in Fig. 3. The optimal knots in the span to include for predicting MOE were within 85% of the span ($Knot\%_{MOE}$). As the percent of span increased from 33 to 85% there was a gradual increase in the coefficient of determination for the linear model. Following the peak reached at 85%, there was a gradual decline in the coefficient of determination. For MOR, the results were clearer in that the linear model results increased from 33 to 65% of the span ($Knot\%_{MOR}$), and then showed a decline after the peak was reached at 65% of the span. In both cases, these results may be specific to the samples used here and thus caution should be exercised when applying these results to the entire population of southern pine lumber. Nevertheless, Knot% values optimized for MOE ($Knot\%_{MOE}$) and MOR ($Knot\%_{MOR}$) were calculated, where $Knot\%_{MOE}$ included the knots located in 85% of the span, and $Knot\%_{MOR}$ included the knots located in 65% of the span. As expected, the different measurements of Knot% were positively correlated with each other, and negatively correlated with SG, AV^2, MOE, and MOR, per the Pearson correlation coefficients (R). For the properties that can be assessed nondestructively, the highest correlation to MOE was with SG (R = 0.78), which was better than AV^2 (R = 0.66) and Knot% (R = −0.55), with $Knot\%_{MOE}$ (R = −0.57) slightly improving on the correlation compared to Knot%. As expected, calculating dynamic MOE (MOE_{dyn}) using SG and AV^2 resulted in improved correlations to MOE (R = 0.82) and MOR (R = 0.74) versus either single parameter. The highest correlation to MOR with a single variable was with $Knot\%_{MOR}$ (R = −0.66) and

Table 3 Pearson correlation matrix among wood properties measured, all coefficients were statistically significant ($\alpha < 0.05$)

Property	$Knot\%_{MOE}$	$Knot\%_{MOR}$	SG	AV^2	MOE_{dyn}	MOE	MOR
Knot%	0.91	0.85	−0.52	−0.51	−0.60	−0.55	−0.63
$Knot\%_{MOE}$		0.91	−0.48	−0.54	−0.60	−0.57	−0.64
$Knot\%_{MOR}$			−0.42	−0.51	−0.55	−0.53	−0.66
SG				0.43	0.75	0.78	0.66
AV^2					0.91	0.66	0.62
MOE_{dyn}						0.82	0.74
MOE							0.78

Knot% percentage of wood made up of knots on the wide faces, $Knot\%_{MOE}$ Knot% optimized for MOE using 85% of the span, $Knot\%_{MOR}$ Knot% optimized for MOR using 65% of the span, *SG* specific gravity, AV^2 acoustic velocity squared, MOE_{dyn} dynamic modulus of elasticity, *MOE* static modulus of elasticity, *MOR* modulus of rupture

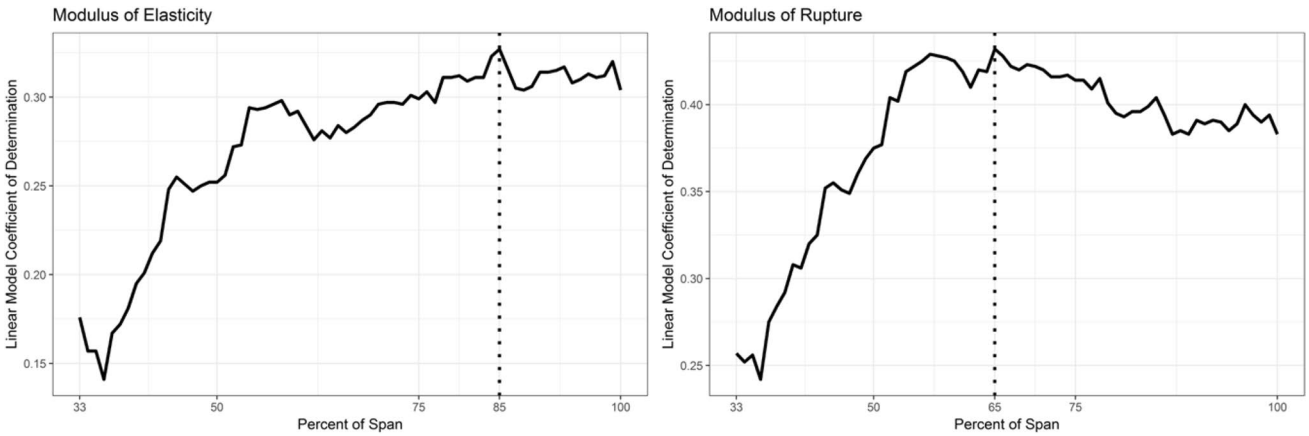

Fig. 3 Selection of the optimal amount of the span to include in the knot area ratio measurement to improve modulus of elasticity and modulus of rupture predictions. Note that 33% is the amount of span associated with the load heads and 100% is the entire span

SG (R = 0.66), which had a slight improvement over Knot% (R = − 0.63), and AV^2 (R = 0.62).

3.2 Summary statistics and comparison between wood properties by failure cause

Summary statistics for the relevant variables are presented in Table 4. Of the 171 pieces in the study, 52 failed in clear wood, 86 failed as a result of a single knot, and 33 failed as a result of a combination of knots (i.e., 2 or more knots in close proximity). The ANOVA results show statistically significant differences between the means of the Knot%, SG, AV^2, MOE_{dyn}, MOE, and MOR due to failure type; the distributions of data points for MOE and MOR by reason of failure are shown in boxplots (Fig. 4). For all variables, clear wood failure was always significantly different from that by a single knot or by multiple knots. Failure by a single knot was not significantly different from failure by multiple knots except for $Knot\%_{MOE}$, $Knot\%_{MOR}$, and MOR. Not surprising here is that the clear wood failures occur in wood that has higher mechanical properties, coinciding with higher SG (0.54), AV^2 (22 $km^2\ s^{-2}$) and MOE_{dyn} (12.1 GPa) and lower Knot% values; this could be attributed to the pieces being from the outerwood, whereas corewood would have lower SG, AV^2, MOE_{dyn}, and larger Knot%. The boxplots show that failure at a single knot had a slightly lower minimum value for MOE and MOR compared to failure at clearwood, whereas failure because of multiple knots had much lower minimum values for both MOE and MOR.

3.3 Modeling modulus of elasticity and modulus of rupture

Single and multiple linear regression models are shown in Table 5 for both MOE and MOR. The plots of MOE are shown in Fig. 5. For the prediction of MOE, Knot% explained 30% of the variation (RMSE = 1.9 GPa). Optimizing the knots included in the Knot% measurement ($Knot\%_{MOE}$) resulted in a slightly improved prediction of MOE ($R^2 = 0.32$, RMSE = 1.9 GPa). Both SG ($R^2 = 0.6$, RMSE = 1.4 GPa) and AV^2 ($R^2 = 0.44$, RMSE = 1.7 GPa) were more accurate at predicting MOE than the Knot%

Table 4 Summary statistics for all lumber and by failure cause

Failure cause	Statistic	Knot%	$Knot\%_{MOE}$	$Knot\%_{MOR}$	SG	AV^2	MOE_{dyn}	MOE	MOR
Overall N = 171	Mean	0.9	0.9	0.9	0.51	21	10.9	10.6	39.2
	Min	0	0	0	0.41	13	6.4	4.5	12.7
	Max	2.4	2.6	3.1	0.64	31	18.6	17.5	72.8
	Std	0.5	0.5	0.6	0.05	3	2.3	2.3	12.3
Clear wood N = 52	Mean	0.6a	0.6a	0.5a	0.54a	22a	12.1a	11.6a	46.6a
	Min	0	0	0	0.44	15	7.7	7.3	24.5
	Max	1.8	1.9	2.2	0.64	29	16.8	15.6	72.8
	Std	0.4	0.4	0.4	0.05	3	2.4	2.1	12.1
Single knot N = 86	Mean	1b	0.9b	0.9b	0.51b	21b	10.6b	10.5b	37.6b
	Min	0.3	0.2	0.1	0.41	13	6.4	6.4	20.4
	Max	2.4	2.5	2.9	0.63	31	18.6	17.5	64.1
	Std	0.5	0.5	0.5	0.05	3	2.2	2.2	10.6
Multiple knots N = 33	Mean	1.1b	1.2c	1.3c	0.49b	20b	10.0b	9.4b	32c
	Min	0.3	0.4	0.3	0.44	16	7.2	4.5	12.7
	Max	2	2.6	3.1	0.57	26	14.6	13.8	54.2
	Std	0.5	0.5	0.6	0.04	3	1.9	2.3	11

Knot% percentage of wood made up of knots on the wide faces, $Knot\%_{MOE}$ Knot% optimized for MOE using 85% of the span, $Knot\%_{MOR}$ Knot% optimized for MOR using 65% of the span, *SG* specific gravity, AV^2 acoustic velocity squared ($km^2\ s^{-2}$), MOE_{dyn} dynamic modulus of elasticity (GPa), *MOE* static modulus of elasticity (GPa), *MOR* modulus of rupture (MPa). Letters denote significant differences ($\alpha < 0.05$) in each column by Tukey test due to failure type

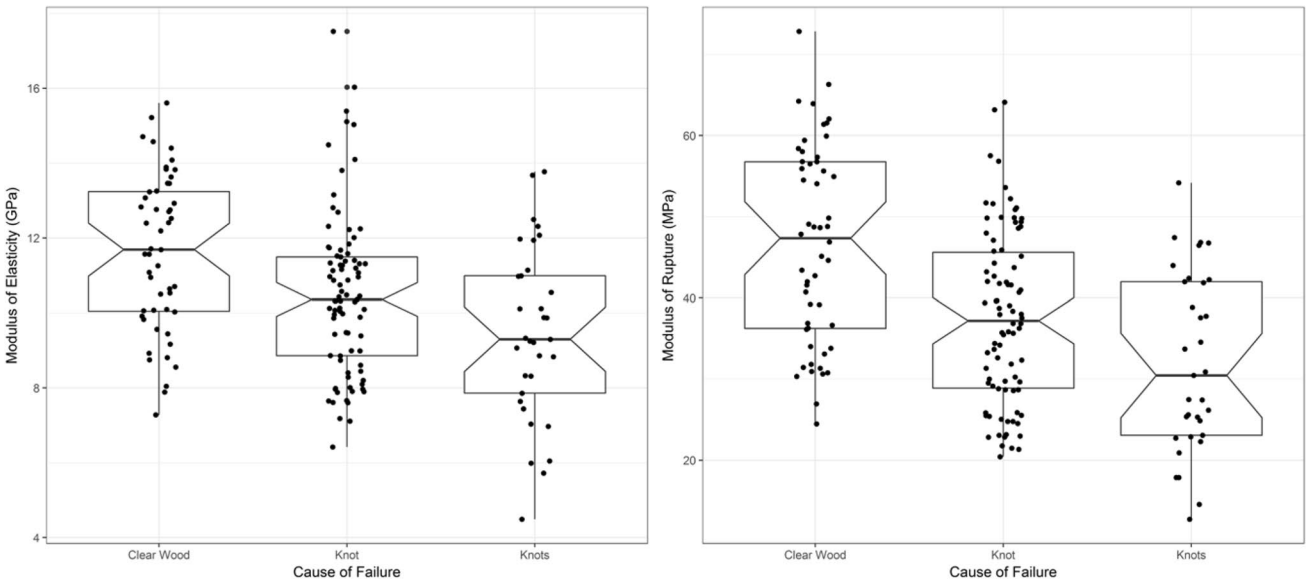

Fig. 4 Boxplots of modulus of elasticity and modulus of rupture by reason of failure where lumber failed in clear wood, at a knot, or at multiple knots (≥2). The boxplots show each data point, the first quartile (or first quantile to be consistent with Table 1), median and the 95% confidence interval of the median, and the third quartile

measurements. The base model of SG and AV^2 explained 74% of the variation in MOE and had a RMSE of 1.2 GPa. Adding Knot% to this base model did not result in an improved model (not shown in table because not significant). Adding $Knot\%_{MOE}$ to the base model in place of Knot% resulted in the $Knot\%_{MOE}$ term to be significant, and a significantly better model determined using ANOVA compared to the base model ($p = 0.025$), however the prediction statistics for the models were nearly identical (RMSE = 1.1 GPa) and the variation explained only increased by 1% ($R^2 = 75\%$). Thus, it was felt the results were not practically significant. Calculating MOE_{dyn} from

Table 5 Regression parameters for linear models using modulus of elasticity and modulus of rupture as the dependent variables

Model		Regression statistics		Model parameters			
y	Equation	R^2	RMSE	β_0	β_1	β_2	β_3
MOE (GPa)	$\beta_0+\beta_1$Knot%	0.30	1.9	14.8	−4.6		
	$\beta_0+\beta_1$Knot%$_{MOE}$	0.32	1.9	14.6	−4.5		
	$\beta_0+\beta_1$SG	0.60	1.4	−8.1	36.4		
	$\beta_0+\beta_1AV^2$	0.44	1.7	0.8	0.5		
	$\beta_0+\beta_1MOE_{dyn}$	0.68	1.3	1.7	0.8		
	$\beta_0+\beta_1SG+\beta_2AV^2$	0.74	1.2	−10.1	28.5	0.3	
	$\beta_0+\beta_1$Knot% $+\beta_2MOE_{dyn}$	0.69	1.3	3.2	−0.9	0.8	
	$\beta_0+\beta_1$Knot%$_{MOE}+\beta_2MOE_{dyn}$	0.69	1.3	3.4	−1.0	0.7	
	$\beta_0+\beta_1$Knot%$_{MOE}+\beta_2SG+\beta_3AV^2$	0.75	1.1	−7.9	−0.8	27.0	0.3
MOR (MPa)	$\beta_0+\beta_1$Knot%	0.39	9.6	64.4	−27.9		
	$\beta_0+\beta_1$Knot%$_{MOR}$	0.43	9.2	62.2	−26.3		
	$\beta_0+\beta_1$SG	0.43	9.2	−46.1	166.0		
	$\beta_0+\beta_1AV^2$	0.38	9.6	−10.2	2.3		
	$\beta_0+\beta_1MOE_{dyn}$	0.54	8.4	−3.1	3.9		
	$\beta_0+\beta_1SG+\beta_2AV^2$	0.56	8.0	−56.5	121.8	1.6	
	$\beta_0+\beta_1$Knot% $+\beta_2MOE_{dyn}$	0.59	7.9	18.7	−13.1	3.0	
	$\beta_0+\beta_1$Knot%$_{MOR}+\beta_2MOE_{dyn}$	0.63	7.5	21.0	−14.5	2.8	
	$\beta_0+\beta_1$Knot% $+\beta_2SG+\beta_3AV^2$	0.61	7.6	−25.8	−11.9	97.0	1.2
	$\beta_0+\beta_1$Knot%$_{MOR}+\beta_2SG+\beta_3AV^2$	0.65	7.2	−21.1	−14.3	100.0	1.0

Knot% percentage of area with knots determined using actual area, *Knot%$_{MOE}$* Knot% optimized for MOE using 85% of the span, *Knot%$_{MOR}$* Knot% optimized for MOR using 65% of the span, *SG* specific gravity, *AV*^{2} acoustic velocity squared (km^2 s^{-2}), *MOE$_{dyn}$* dynamic modulus of elasticity (GPa), *MOE* static modulus of elasticity (GPa), *MOR* modulus of rupture (MPa)

SG and AV^2 resulted in a decrease in model performance ($R^2=0.68$, 1.3 GPa) over the base model, with similar performance decreases when also adding Knot% or Knot%$_{MOE}$ to the MOE$_{dyn}$ model.

The plots of MOR are shown in Fig. 6. For the prediction of MOR, Knot% explained 39% of the variation (RMSE = 9.6 MPa). Optimizing the knots included in the Knot% measurement (Knot%$_{MOR}$) resulted in a slightly improved prediction of MOR ($R^2=0.43$, RMSE = 9.2 MPa). For the prediction of MOR, Knot%$_{MOR}$ was identical to the accuracy of SG model ($R^2=0.43$, RMSE = 9.2 MPa) and both were better than AV^2 ($R^2=0.38$, RMSE = 9.6 MPa). The base model of SG and AV^2 explained 56% of the variation in MOR with a RMSE of 8.0 MPa. Adding Knot% to this base model resulted in an improved model with $R^2=0.61$ and RMSE = 7.6 MPa, which was further improved by replacing it with Knot%$_{MOR}$ ($R^2=0.65$, RMSE = 7.2 MPa). The base model of SG and AV^2 had improved performance over the model with MOE$_{dyn}$.

The image analysis approach used here demonstrated the ability to quantify knots using equipment that is considerably less expensive than other systems (e.g., X-ray scanners). Only images of the wide faces were captured, which is comparable to how X-ray scanning equipment functions; this differs from measurements involving the tracheid effect, which typically captures images on all four sides of the lumber. While the differences in equipment are notable, of specific interest was whether knot information obtained via RGB images would be sufficient to improve the mechanical property predictions using SG and AV^2 alone.

Results presented here show that knot information (e.g., Knot%) is particularly helpful in improving the prediction of MOR, with the prediction of MOE not appreciably improving over models constructed using SG and AV^2 alone. Recently, França et al. (2018) modeled MOE and MOR for southern pine, with dynamic MOE calculated using transverse vibration. They calculated the knot depth ratio (KDR, i.e. knot thickness/lumber thickness) and knot area ratio (KAR, i.e. in cross section, knot area divided by total area); these properties were determined through manual measurement by cutting open the cross section at the failure point and evaluating the knots within a 15 cm length. They found weaker relationships between knot depth ratio and both MOE ($R^2=0.13$) and MOR ($R^2=0.2$) than reported here for the various Knot% measurements. They did find stronger relationships between dynamic MOE and MOE ($R^2=0.84$) than here with SG and AV^2 ($R^2=0.74$). While this could simply be due to the samples tested, it is likely due to their determination of dynamic MOE via transverse vibration which is more accurate than using wood density and AV^2

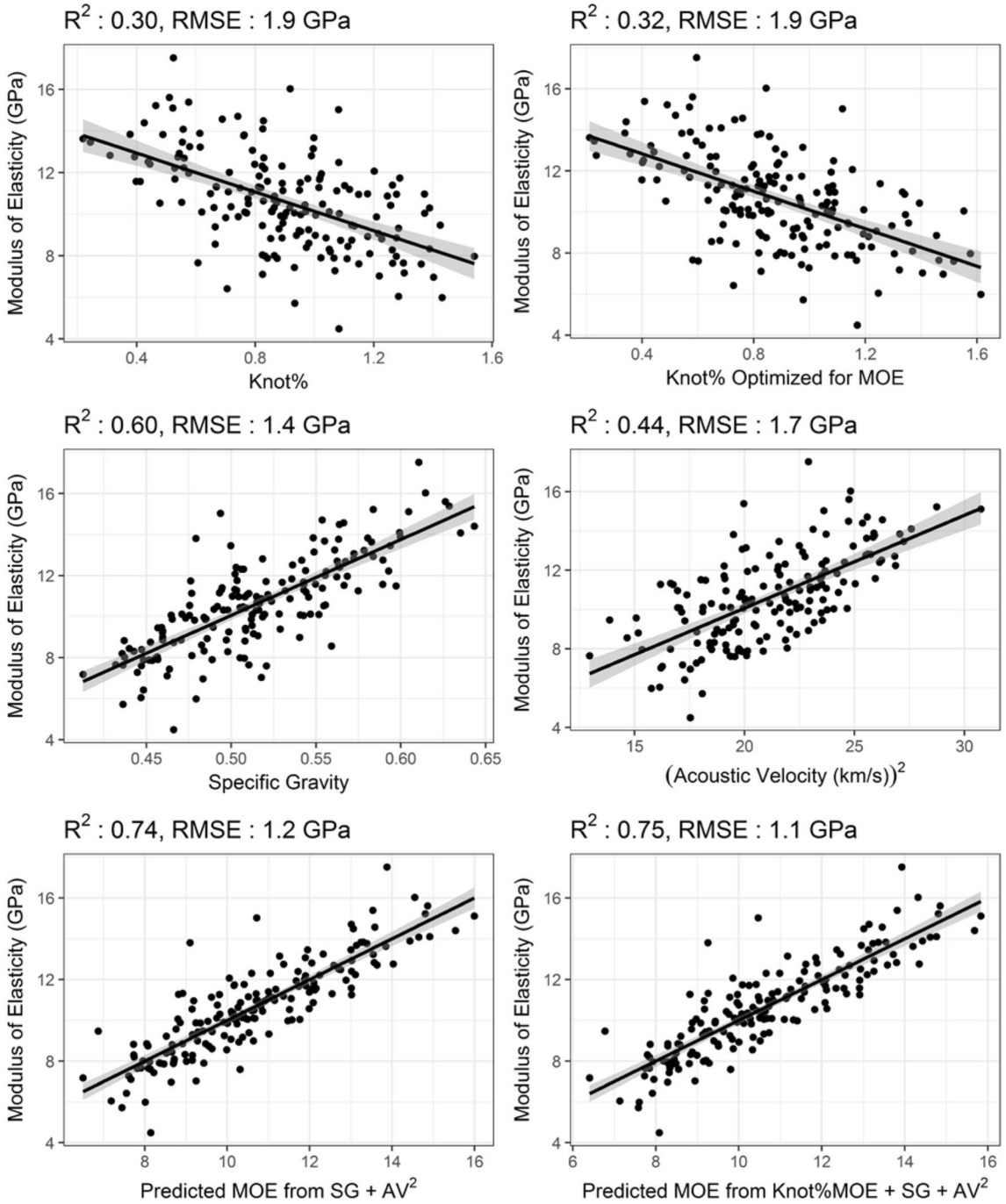

Fig. 5 Single and multiple linear relationships between static modulus of elasticity (MOE) and Knot%, Knot% optimized for MOE, specific gravity (SG), and acoustic velocity squared (AV^2). The regression line (solid black line) is shown along with the 95% confidence interval of the mean (gray polygon around black line)

(Viguier et al. 2017; Dahlen et al. 2018). The present results also show that improved predictions can be found by fitting a multiple regression model using SG and AV^2 versus calculating MOE_{dyn} from the two parameters. It should be noted that knot depth ratio can be reasonably estimated using density measurements determined using X-ray radiation (Oh et al. 2009); while this measurement method is amenable to automation, obstacles do exist with regard to cracks in the knots which gives underestimates of density, and thus can underestimate the knot depth ratio.

The results found here using the combined model with SG, AV^2, and Knot% (or $Knot\%_{MOR}$) gave similar coefficient

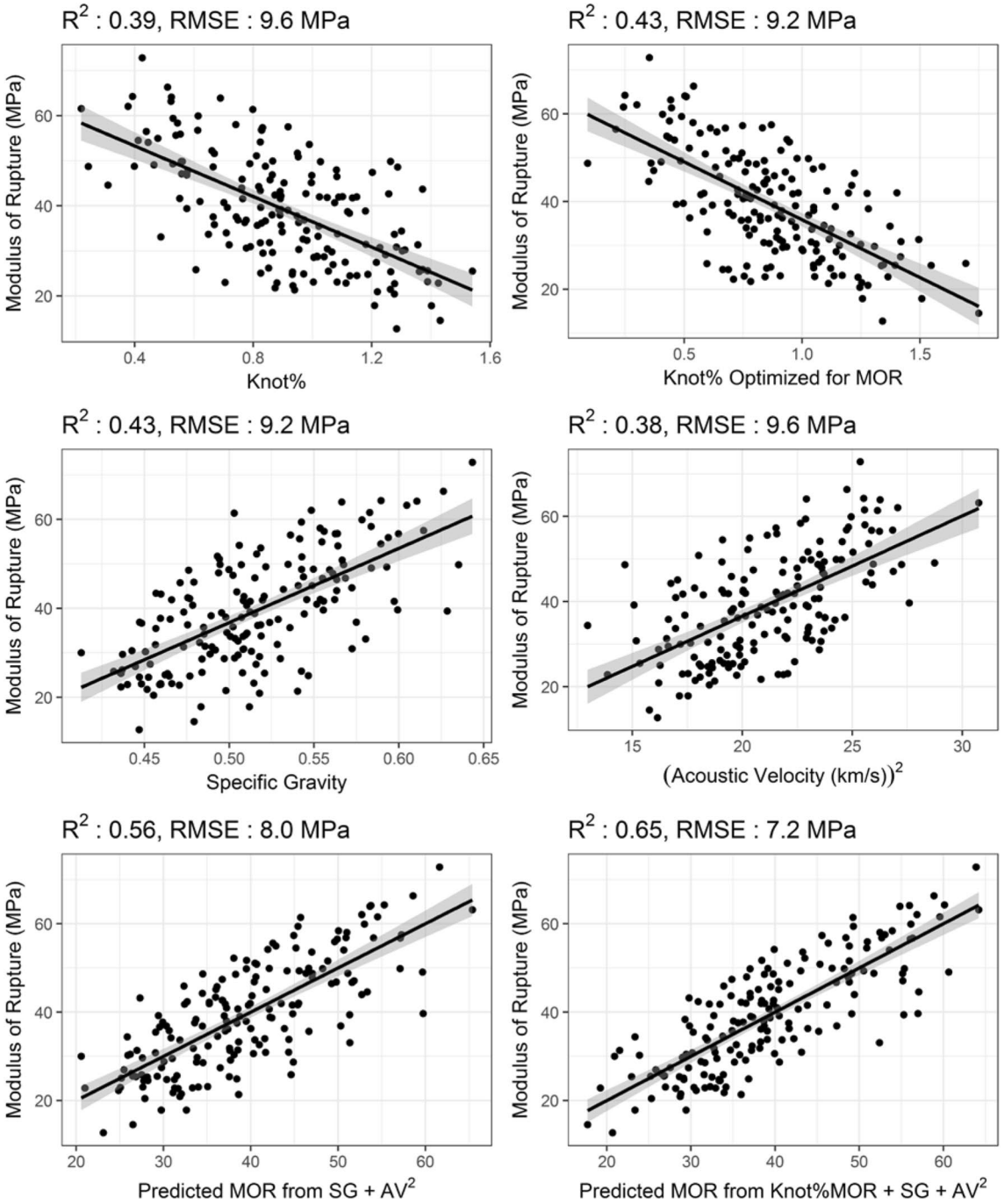

Fig. 6 Single and multiple linear relationships between modulus of rupture (MOR) and Knot%, Knot% optimized for MOR, specific gravity (SG), and acoustic velocity squared (AV^2). The regression line (solid black line) is shown along with the 95% confidence interval of the mean (gray polygon around black line)

of determination values ($R^2 = 0.57–0.65$) to those of Schajer (2001) with southern pine tested in bending, specifically, between MOR and predicted MOR. Similar to Oh et al. (2009), Schajer (2001) determined knots using an X-ray system; however, the density values were not used to determine values for knot depth ratio, but instead, the estimate for MOR was determined by multiplying the clear wood MOR by a structural factor based on locally high density values corresponding to knots. What is not known is whether an image based system would improve MOE and/or MOR predictions in lumber sizes greater than those tested here, such as the 2 × 10 (38.1 mm × 235 mm) and 2 × 12

(38.1 mm × 285.8 mm) sizes. It is noted that the Schajer (2001) study utilized a much larger sample size (N = 605) than employed here (N = 171), and they found some variability in the results based on the samples tested, being from three different mills.

The results presented here are also similar to the results that others have found in various softwood species using both X-ray scanning equipment (Lam et al. 2004, 2005; Oh et al. 2008) and equipment that measures the tracheid effect (Roblot et al. 2010; Olsson et al. 2013; Viguier et al. 2017; Olsson et al. 2018). To the authors' knowledge, no published study exists for southern pine lumber using the tracheid effect. This makes it difficult to make comparisons between the tracheid effect technique and the results presented here using image analysis for southern pine lumber due to species differences. Specifically, much of the work published on the tracheid effect has focused on Norway spruce and Douglas-fir, with the mechanical properties for spruce being predicted with greater accuracy than Douglas-fir, likely due to the large knots in Douglas-fir (Viguier et al. 2017; Olsson et al. 2018). Expanding the comparison to hardwoods results in even more variability, with very different relationships obtained depending on the particular species. For example, Nocetti et al. (2017) found in *Eucalyptus grandis* (N = 130) that dynamic MOE was a much better predictor of MOR ($R^2 = 0.36$) than a knot parameter ($R^2 = 0.06$); where knot information was determined through an algorithm combining knot position and relative size information using both the tracheid effect and X-ray information. In the case of European oaks (*Quercus petraea* and *Quercus robur*) (N = 470) the opposite has been found, whereby dynamic MOE had a poor relationship with bending strength ($R^2 = 0.22$) versus local fiber orientation found using the tracheid effect ($R^2 = 0.59$) (Olsson et al. 2018).

Commercial scanning systems that employ either X-rays, or differentiate knots using the tracheid effect, have been successfully used by numerous researchers (Schajer 2001; Oh et al. 2008; Roblot et al. 2010; Olsson et al. 2013; Viguier et al. 2017) to improve prediction of mechanical properties. While the current technique is not suitable for commercial operations that require online scanning of speeds up to 450 m min^{-1} (Olsson and Oscarsson 2017), it is relatively inexpensive to deploy in a laboratory setting. Notwithstanding, it is acknowledged that to augment image quality between the clearwood and the knots, which increased the capacity to measure Knot% values, necessitated the delineation of the knots from the clearwood using a marker. The technique described herein also captures the lumber image in a single image. A custom-built scanner is currently being constructed and will image each side multiple times which will also allow for greater resolution to further enhance the knot detection efforts. One possible solution for delineating knots from clearwood without the use of a marker is through machine learning techniques which have proven useful in knot identification (Cavalin et al. 2006), apart from a multitude of other applications including wood identification (Yadav et al. 2017). Future work will also concentrate on collecting knot information on all four faces. Collecting information on all four sides will allow for the quantification of knot area ratio on the cross-sectional face and will allow the technique to be more comparable to results from studies utilizing the tracheid effect (Roblot et al. 2010; Olsson et al. 2013; Viguier et al. 2017; Olsson et al. 2018). Capturing images on all four sides could also allow for modeling of knots towards the pith following the work on Norway spruce using the tracheid effect (Briggert et al. 2016; Hu et al. 2018b; Lukacevic et al. 2019).

As noted in Olsson et al. (2013) and explored further by Hu et al. (2018a), grain angle changes due to knots is an interesting research question. Measuring the tracheid effect offers the opportunity to quantify the changes in grain direction specific to the knot itself versus the impacts that the knots have on the localized slope of grain. Ehrhart et al. (2018) recently used image analysis techniques to measure the grain angle in European beech (*Fagus sylvatica* L.) by detecting the orientation of the rays relative to the longitudinal surface. For hardwood species with visible rays this technique seems suitable for laboratory measurement of grain angle changes. For softwoods however, measuring the localized slope of grain surrounding the knots using image analysis on RGB images would likely not be feasible.

Regardless of the technique employed to quantify knots, an improved understanding of their particular impact on lumber is needed. Branch size and distribution within wood available in commerce is changing as more material worldwide is sourced from fast grown plantations that are planted at lower planting densities (Auty et al. 2012). In addition to changes in the knots, the wood from these trees will be made up of a higher proportion of lower stiffness and strength corewood (Burdon et al. 2004; Lachenbruch et al. 2011; Moore and Cown 2017). The recent decline in the design values for visually graded southern pine lumber illustrates the importance of better forecasting changes. One opportunity is to incorporate wood quality into forest growth and yield systems (Mäkinen and Colin 1998). Combining models of wood and fiber properties with branch structure (Duchateau et al. 2013; Osborne and Maguire 2016), and incorporating them into growth and yield systems would allow forest managers to project growth and internal properties. Ideally these systems will have capabilities whereby trees can be "virtually grown" and then bucked into logs and sawn (Mäkelä et al. 2010). The predicted internal properties could then be used to predict the MOE and MOR of the lumber to enable predictions of the conformance of the wood to product specifications. The work assessing knots in lumber is an important part of this modeling chain.

4 Conclusion

A process to conduct cost-efficient knot analysis in a laboratory setting to predict the mechanical properties of lumber is presented. Image analysis of loblolly pine lumber RGB images was conducted on the wide faces of the lumber from a mill study using *k*-means clustering to identify knots, which were then delineated from the clear wood. The Knot%, calculated on the basis of the actual knot area of the wide faces, improved the prediction models for the mechanical properties, with MOE and MOR decreasing with increasing Knot%. The best MOE model included knots from within 85% of the test span, while the best MOR model included knots from 65% of the span. Knot% measurements did not appreciably improve static MOE predictions compared to the base SG and acoustic velocity model, but they did significantly improve MOR predictions. These conclusions are specific to this dataset, which only included 2×6 and 2×8 material; however, the method generated here could be used by laboratories that are not equipped with traditional knot scanning equipment to assess the impacts that knots have on the mechanical properties of lumber. More information is needed on a broader sample size that links the knot information with common measurements of lumber quality including grade, specific gravity, and acoustic velocity to determine the specific knot parameters (e.g., size, location, shape) that most negatively impact mechanical properties. The knot quantification technique could also be used to determine the impacts that silvicultural treatments, such as pruning and thinning intensity, have on the knot sizes in lumber.

Acknowledgements This research was possible through support from the National Science Foundation (NSF) (No. 1361755) Center for Advanced Forest Systems (CAFS), the Wood Quality Consortium (WQC) at the University of Georgia, the Plum Creek Timber Company (now Weyerhaeuser), and the NIFA McIntire-Stennis Project 1006098. The authors wish to thank NSF CAFS, the WQC, Plum Creek Timber Company (now Weyerhaeuser), and NIFA for funding this project. We also gratefully acknowledge Varn Wood Products LLC., who processed the logs into structural lumber in their sawmill. Finally, we would like to thank the two anonymous reviewers and the editor for their helpful comments and suggestions in improving the manuscript.

Compliance with ethical standards

Conflict of interest The authors declare that they have no competing interests.

References

ASTM D198-15 (2015) Standard test methods of static tests of lumber in structural sizes. ASTM International, West Conshohocken

ASTM D1990-16 (2016) Standard practice for establishing allowable properties for visually-graded dimension from in-grade tests of full-size specimens. ASTM International, West Conshohocken

ASTM D245-11 (2011) Standard practice for establishing structural grades and related allowable properties for visually-graded dimension. ASTM International, West Conshohocken

ASTM D4761-13 (2013) Standard test methods for mechanical properties of lumber and wood-base structural material. ASTM International, West Conshohocken

Auguie B (2016) gridExtra: Miscellaneous functions for "grid" graphics. R package version 2.2.1. https://CRAN.R-project.org/package=gridExtra. Accessed 1 Nov 2018

Auty D, Weiskittel AR, Achim A, Moore JR, Gardiner BA (2012) Influence of early re-spacing on Sitka spruce branch structure. Ann For Sci 69:93–104

Bivand R, Rundel C (2017) rgeos: interface to geometry engine- open source (GEOS). R package version 0.3-23. https://cran.rstudio.com/web/packages/rgeos/rgeos.pdf. Accessed 1 Nov 2018

Bivand R, Keitt T, Rowlingson B (2017) rgdal: bindings for the geospatial data abstraction library. R package version 1.2-7. https://cran.r-project.org/web/packages/rgdal/rgdal.pdf. Accessed 1 Nov 2018

Bradski G (2000) The OpenCV Library. Dr. Dobb's J Softw Tools. 2236121

Briggert A, Olsson A, Oscarsson J (2016) Three-dimensional modelling of knots and pith location in Norway spruce boards using tracheid-effect scanning. Eur J Wood Prod 74:725–739

Briggert A, Hu M, Olsson A, Oscarsson J (2018) Tracheid effect scanning and evaluation of in-plane and out-of-plane fiber direction in Norway spruce timber. Wood Fib Sci 50(4):411–429

Brownrigg R (2016) maps: draw geographical maps. R package version 3.1.1. https://cran.r-project.org/web/packages/maps/maps.pdf. Accessed 1 Nov 2018

Burdon RD, Kibblewhite RP, Walker JCF, Megraw RA, Evans R, Cown DJ (2004) Juvenile versus mature wood: a new concept, orthogonal to corewood versus outerwood, with special reference to *P. radiata* and *P. taeda*. For Sci 50(4):399–415

Butler MA, Dahlen J, Daniels RF, Eberhardt TL, Antony B (2016) Bending strength and stiffness of loblolly pine lumber from intensively managed stands located on the Georgia Lower Coastal Plain. Eur J Wood Prod 74(1):91–100

Butler MA, Dahlen J, Eberhardt TL, Montes C, Antony F, Daniels RF (2017) Acoustic evaluation of loblolly pine tree and lumber-length logs allows for segregation of modulus of elasticity, not modulus of rupture. Ann For Sci 74:20

Cavalin P, Oliveira LS, Koerich AL, Britto Jr AS (2006) Wood defect detection using grayscale images and an optimized feature set. In: Proc IEEE Ind Electron (IECON 2006), pp 3408–3412

Clark A III, Jordan L, Schimleck L, Daniels RF (2008) Effect of initial planting spacing on wood properties of unthinned loblolly pine at age 21. For Prod J 58(10):78–83

Cramer S, Kretschmann D, Lakes R, Schmidt T (2005) Earlywood and latewood elastic properties in loblolly pine. Holzforschung 59(5):531–538

Dahlen J, Montes C, Eberhardt TL, Auty D (2018) Probability models that relate nondestructive test methods to lumber design values of plantation loblolly pine. Forestry 91(3):295–306

Duchateau F, Longuetaud F, Mothe F, Ung C, Auty D, Achim A (2013) Modelling knot morphology as a function of external tree and branch attributes. Can J For Res 43:266–277

Ehrhart T, Steiger R, Frangi A (2018) A non-contact method for the determination of fibre direction on European beech wood (*Fagus sylvatica* L.). Eur J Wood Prod 76:925–935

Evans JW, Kretschmann DE, Herian VL, Green DW (2001) Procedures for developing allowable properties for a single species under

ASTM D1990 and computer programs useful for the calculations. USDA Forest Service. Forest Products Laboratory. FPL-GTR-126
Fox TR, Jokela EJ, Allen HL (2007) The development of pine plantation silviculture in the southern United States. J For 105(7):337–347
França FJN, Seale RD, Shmulsky R, França TSFA (2018) Modeling mechanical properties of 2×4 and 2×6 southern pine lumber using longitudinal vibration and visual characteristics. Forest Prod J **(in press)**
Glass SV, Zelinka SL (2010) Moisture relations and physical properties of wood. In: Wood Handbook. Gen Tech Rep FPL-GTR-190. Ed. Ross, R.J. U.S. Department of Agriculture, Forest Service, Forest Products Laboratory, Madison, pp 4-1–4-19
Hartigan JA, Wong MA (1979) A K-means clustering algorithm. Appl Stat 28(1):100–108
Hartley R, Zisserman A (2003) Multiple view geometry in computer vision. Cambridge University Press, Cambridge
Hijams RJ (2016) raster: geographic data analysis and modeling. R package version 2.5-8. https://cran.r-project.org/web/packages/raster/raster.pdf. Accessed 1 Nov 2018
Hu M, Briggert A, Olsson A, Johansson M, Oscarsson J, Säll H (2018a) Growth layer and fibre orientation around knots in Norway spruce: a laboratory investigation. Wood Sci Technol 52:7–27
Hu M, Olsson A, Johansson M, Oscarsson J (2018b) Modelling local bending stiffness based on fibre orientation in sawn timber. Eur J Wood Prod 76:1605–1621
Jokela EJ, Martin TA, Vogel JG (2009) Twenty-five years of intensive forest management with southern pines: important lessons learned. J For 108(7):338–347
Jordan L, He R, Hall DB, Clark A III, Daniels RF (2007) Variation in loblolly pine ring microfibril angle in the southeastern United States. Wood Fibre Sci 39(2):352–363
Kanungo T, Netanyahu NS, Wu AY (2002) An efficient k-means clustering algorithm: analysis and implementation. IEEE Trans Pattern Anal 24(7):881–892
Lachenbruch B, Moore JR, Evans R (2011) Radial variation in wood structure and function in woody plants, and hypotheses for its occurrence. In: Meinzer FC, Lachenbruch B, Dawson TE (eds) Size- and age-related changes in tree structure and function. Springer, Berlin, pp 121–164
Lam F, Barrett JD, Nakajima S (2004) Influence of knot area ratio based grading rules on the engineering properties of Hem-fir used in Japanese post and beam housing. Wood Sci Technol 38(2):83–92
Lam F, Barrett JD, Nakajima S (2005) Influence of knot area ratio on the bending strength of Canadian Douglas fir timber used in Japanese post and beam housing. J Wood Sci 51(1):18–25
Larson PR, Kretschmann DE, Clark III A, Isebrands JG (2001) Formation and properties of juvenile wood in southern pines. US For Serv. Forest Products Laboratory. FPL-TR-129
Lukacevic M, Kandler G, Hu M, Olsson A, Füssl J (2019) A 3D model for knots and related fiber deviations in sawn timber for prediction of mechanical properties of boards. Mater Des 166:107617
Madsen B (1992) Structural behavior of timber, 1st edn. Timber Engineering. Print, North Vancouver
Mäkelä A, Grace JC, Deckmyn G, Kantola A, Campioli M (2010) Simulating wood quality in forest management models. For Syst 19:48–68
Mäkinen H, Colin F (1998) Predicting branch angle and branch diameter of Scots pine from usual tree measurements and stand structural information. Can J For Res 28:1686–1696
McKinney W (2010) Data structures for statistical computing in Python. In: Proceedings of the 9th Python in science conference, pp 51–56. http://conference.scipy.org/proceedings/scipy2010/mckinney.html. Accessed 1 Nov 2018
Moore JR, Cown D (2017) Corewood (juvenile wood) and its impact on wood utilisation. Curr For Rep 3(2):107–118
Nocetti M, Pröller M, Brunetti M, Dowse GP, Wessels CB (2017) Investigating the potential of strength grading green *Eucalyptus grandis* lumber using multi-sensor technology. BioResources 12(4):9273–9286
Oh JK, Kim KM, Lee JJ (2008) Development of knot quantification method to predict strength using X-ray scanner. J Korean Wood Sci Technol 36(5):33–41
Oh JK, Shim K, Kim KM, Lee JJ (2009) Quantification of knots in dimension lumber using a single pass X-ray radiation. J Wood Sci 55:264–272
Oliphant TE (2006) A guide to NumPy. Trelgol Publishing, USA
Olsson A, Oscarsson J (2017) Strength grading on the basis of high resolution laser scanning and dynamic excitation: a full scale investigation of performance. Eur J Wood Prod 75:17–31
Olsson A, Oscarsson J, Johansson M, Källsner B (2012) Prediction of timber bending strength on basis of bending strength and material homogeneity assessed from dynamic excitation. Wood Sci Technol 46:667–683
Olsson A, Oscarsson J, Serrano E, Källsner B, Johansson M, Enquist B (2013) Prediction of timber bending strength and in-member cross-sectional stiffness variation on the basis of local wood fibre orientation. Eur J Wood Prod 71:319–333
Olsson A, Guillaume Pot, Viguier J, Faydi Y, Oscarsson J (2018) Performance of strength grading methods based on fibre orientation and axial resonance frequency applied to Norway spruce (*Picea abies* L), Douglas-fir (*Pseudotsuga menziesii* (Mirb.) Franco) and European oak (*Quercus petraea* (Matt.) Liebl./*Quercus robur* L.). Ann For Sci 75:102
Osborne NL, Maguire DA (2016) Modeling knot geometry from branch angles in Doulgas-fir (*Pseudotsuga menziesii*). Can J For Res 46:215–224
Pebesma E, Bivand R (2016) sp: classes and methods for spatial data. R package version 1.2-4. https://cran.r-project.org/web/packages/sp/sp.pdf. Accessed 1 Nov 2018
R Core Team (2018) R: a language and environment for statistical computing. R Foundation for Statistical Computing, Vienna
Roblot G, Bléron L, Mériaudeau F, Marchal R (2010) Automatic computation of the knot area ratio for machine strength grading of Douglas-fir and Spruce timber. Eur J Environ Civ Eng 14(10):1317–1332
RStudio (2018) RStudio: integrated development environment for R (Version 3.3.1). Boston
Schajer GS (2001) Lumber strength grading using X-ray scanning. For Prod J 51(1):43–52
Schultz RP (1999) Loblolly-the pine for the twenty-first century. New For 17:71–88
South DB, Harper RA (2016) A decline in timberland continues for several southern yellow pines. J For 114(2):116–124
SPIB (2004) National grading rule for softwood dimension lumber: interpretations. Southern Pine Inspection Bureau, Pensacola. https://blog.spib.org/wp-content/uploads/2017/09/SPIB-NGR-Interpretations-Single-Page.pdf. Accessed 1 Nov 2018
SPIB (2014) Standard grading rules for southern pine lumber, 2014th edn. Southern Pine Inspection Bureau, Pensacola
Todoroki CL, Lowell EC, Dykstra D (2010) Automated knot detection with visual post-processing of Douglas-fir veneer images. Comput Electron Agric 70:163–171
van der Walk S, Schönberger JL, Nunez-Iglesias J, Boulogne F, Warner JD, Yager N, Gouillart E, Yu T, sci-kit image Contributors (2014) scikit-image: image processing in Python. PeerJ 2:e453
Vance ED, Maguire DA, Zalesney RS Jr (2010) Research strategies for increasing productivity of intensively managed forest plantations. J For 108:183–192

Viguier J, Bourreau D, Bocquet JF, Pot G, Bléron L, Lanvin JD (2017) Modelling mechanical properties of spruce and Douglas fir timber by means of X-ray and grain angle measurements for strength grading purpose. Eur J Wood Prod 75:527–541

Wang X (2013) Acoustic measurements on trees and logs: a review and analysis. Wood Sci Technol 47:965–975

Wear DN, Greis JG (2002) Southern forest resource assessment: summary of findings. J For 100(7):6–14

Wickham and Rstudio (2017) tidyverse: Easily install and load the 'tidyverse' R package version 1.2.1. https://cran.r-project.org/web/packages/tidyverse/index.html. Accessed 1 Nov 2018

Yadav AR, Anand RS, Dewal ML, Gupta S (2017) Binary wavelet transform-based completed local binary pattern texture descriptors for classification of microscopic images of hardwood species. Wood Sci Technol 51:909–927

Ying L, Kretschmann DE, Bendtsen BA (1994) Longitudinal shrinkage in fast-grown loblolly pine wood. For Prod J 44(1):58–62

Publisher's Note Springer Nature remains neutral with regard to jurisdictional claims in published maps and institutional affiliations.